First Principles Computational Study of the Active Site of Arginase

ARTICLE *in* PROTEINS STRUCTURE FUNCTION AND BIOINFORMATICS · DECEMBER 2003

Impact Factor: 2.63 · DOI: 10.1002/prot.10572 · Source: PubMed

2 AUTHORS, INCLUDING:

Ivaylo Ivanov
Georgia State University
45 PUBLICATIONS **1,225** CITATIONS

PROTEINS: Structure, Function, and Bioinformatics 54:1–7 (2004)

SHORT COMMUNICATION

First Principles Computational Study of the Active Site of Arginase

Ivaylo Ivanov* **and Michael L. Klein**
Department of Chemistry, University of Pennsylvania, Philadelphia, Pennsylvania

ABSTRACT **Ab initio density functional theory (DFT) methods were used to investigate the structural features of the active site of the binuclear enzyme rat liver arginase. Special emphasis was placed on the crucial role of the second shell ligand interactions. These interactions were systematically studied by performing calculations on models of varying size. It was determined that a water molecule, and not hydroxide, is the bridging exogenous ligand. The carboxylate ligands facilitate the close approach of the Mn (II) ions by attenuating the metal–metal electrostatic repulsion. Of the two metals, Mn_A was shown to carry a larger positive charge. Analysis of the electronic properties of the active site revealed that orbitals involving the terminal Asp234 residue, as well as the flexible μ-1,1 bridging Asp232, lie at high energies, suggesting weaker coordination. This is reflected in certain structural variability present in our models and is also consistent with recent experimental findings. Finally, implications of our findings for the biological function of the enzyme are delineated. Proteins 2004;54:1–7.**

Key words: arginase; second shell ligands; binuclear metalloenzyme; density functional theory; manganese

INTRODUCTION

A wide variety of proteins rely on bimetal cofactors to carry out reactive chemistry. For instance, bridged binuclear metallohydrolases[1] are often involved in phosphate ester and peptide bond hydrolysis, and play a vital role in DNA repair (DNA polymerase, P1 nuclease), hormone regulation (purple acid phosphatase and related enzymes, phospholipase C, alkaline phosphatase), tissue repair, protein maturation, and carcinogenesis (bovine lens leucine aminopeptidase, methionine aminopeptidase, and related enzymes).[2–6] Some prominent examples of redox proteins sharing the same structural motif are methane monooxygenase (MMO), ribonucleotide reductase, and manganese catalase.[7–9] The metal-binding sites of these proteins strike a delicate balance between the requirement for tight binding of the cofactor and the need to undergo dynamic transformations as the reaction proceeds. In the case of hydrolytic enzymes, catalytic action is dependent on the exact positioning and hydrogen-bonding pattern of a number of active site residues, which fine-tune the interaction of the active nucleophile species with the metal centers. In the present study, we have focused on how this fine-tuning is realized in a specific enzyme—rat liver arginase.[10–12] To this end, we have carried out extensive density functional computations aimed at determining the structural and electronic properties of the arginase active site. Such a first principles quantum mechanical (QM) approach can be instrumental in elucidating the details of the active site structure and the nature of catalytic activity.

Arginase catalyzes the hydrolysis of L-arginine to form L-ornithine and urea. This reaction takes place in the liver as the last step of the urea cycle through which nitrogenous substances are metabolized. The proposed reaction mechanism[11,13] (see Fig. 1) involves a nucleophilic attack of a bridging OH^- ion on the guanidinium group of arginine, resulting in the formation of a tetrahedral intermediate. The next step in the catalytic cycle is the collapse of the intermediate following proton transfer through Asp128 to the leaving group (ornithine). The cycle is completed by the release of the products and the regeneration of the active nucleophile. It should be noted that an alternative mechanism was suggested by Khangulov et al.[14] The major points of departure from the above mechanism are (1) initial substrate deprotonation and binding to one of the metals, and (2) nucleophilic attack from a terminal as opposed to bridging position. The fact that chelating agents can be used to extract the more weakly bound manganese atom (Mn_A) to produce a half-active state of the enzyme[11,15] prompted us to examine metal-depleted as well as native active site models.

Grant sponsor: National Science Foundation; Grant number: CHE-0205146.

*Correspondence to: Ivaylo N. Ivanov, Department of Chemistry, University of Pennsylvania, 231 S. 34th Street, Philadelphia, PA. E-mail: iivanov@cmm.chem.upenn.edu

Received 16 March 2003; Accepted 24 June 2003

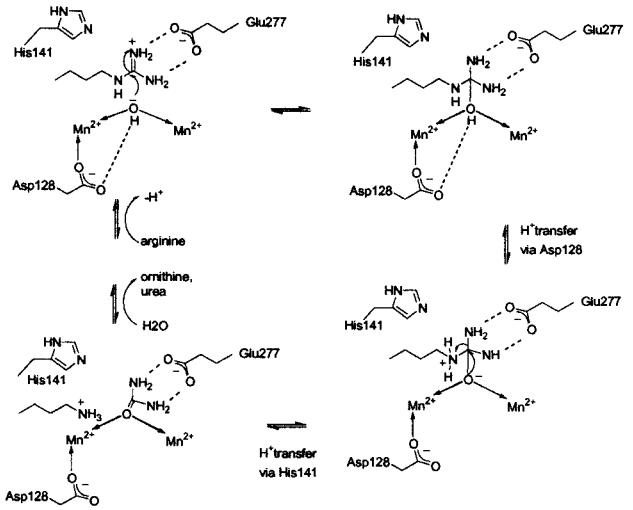

Fig. 1. Mechanism of L-arginine hydrolysis proposed by Christianson et al.[11,13]

Our first goal was to obtain a reliable geometric representation of the active site of rat liver arginase. To accomplish this, we have explored active site models (see Table I) that substantially exceed the system sizes commonly employed in metalloenzyme modeling (at present, approximately 50 or 60 atoms is considered computationally practical). Geometry optimizations of larger transition metal systems at a correlated DFT level are less common due to the considerable computational expenses involved. Nevertheless, we feel that investigation of such systems is worthwhile, as it gives insight into the role of residues removed from immediate contact with the metal centers but crucial in shaping the structure of the active site through hydrogen bonding and/or spatial restraints. To assess the influence of constraints applied during geometry optimization, two types of calculations were performed on the minimal model RLA_h2o: (1) The ligands were anchored at the peptide bond, or (2) all atoms were allowed to relax freely to their equilibrium positions. Comparison of the constrained and unconstrained models using the calculated root-mean-square deviation (RMSD; 0.19 Å, including all hydrogen atoms) reveals that the structures are remarkably similar, with more significant deviations apparent only in the immediate vicinity of the constrained atoms. From all bonds found within the core of the binuclear cluster, the most sensitive to the presence of constraints are those between the manganese atoms (Mn_A; Mn_B) and O* (the oxygen of the bridging exogenous water molecule) ($\Delta d = 0.06$ Å and 0.05 Å, respectively), as well as the bond between Mn_B and the more distant oxygen atom of the flexible terminal Asp234 residue ($\Delta d = 0.04$ Å). This is an indication that the corresponding bonds are the most labile in the structure. The Mn–Mn intermetal distances are, surprisingly, shorter in the absence of constraints by about 0.03 Å—a fact that reflects the strong stabilization effect of the carboxylate ligands on the electrostatic repulsion between the manganese ions. Regarding the energetic effect of constraints, it was not possible to directly estimate it from the RLA_h2o model, because the CO distances in the peptide bonds were fixed. To address this issue, we optimized an additional model with only the peptide carbonyl carbon atoms restrained. The difference in total energies between this model and the unconstrained optimized structure is only 1.25 kcal/mol. Thus, we estimate that the energetic cost of confining the active site within the larger framework of the protein environment is small. In the following discussion, we refer primarily to the constrained models, as they are supposed to better represent the geometry of the active site. Optimized structures for two of the minimal models—RLA_h2o and RLA_dep—are presented in Figure 2. The geometries of the minimal models were determined to agree qualitatively with the crystal structures and results from electron paramagnetic resonance (EPR) and extended absorption fine structure (EXAFS) experiments.[16,17] The EXAFS results were fit with a single low Z (C, O, N) nearest neighbor shell and reveal an average Mn-O/N distance of 2.17 Å with a relatively large Debye–Waller factor. The corresponding average from the X-ray structure is 2.25 Å, with the computational results falling in between at 2.21 Å. The intermetal distances from the crystal structures (about 3.3 Å)[13] and from the analysis of zero field splittings in the EPR spectra (3.36–3.57 Å)[16] should be compared to our calculated values of 3.12–3.45 Å in Table II. As the intermetal distance in the μ-hydroxo bridged model is much shorter than what was found experimentally ($\Delta d =$ 0.20 Å and 0.23 Å), this strongly suggests that the bridging species in the experiments was a water molecule. This observation is further strengthened by examining the $Mn_{A,B}$—O* distances for the water-bridged models (see Table I) and comparing them to the corresponding distances in the hydroxide-bridged models and the X-ray structure. The crystal structure of native arginase[13] was determined at a 2.10 Å resolution. A rough estimate of the uncertainty in the crystallographic Mn7—O* bond lengths can be obtained by looking at these distances in the three identical subunits. The average of all six distances is 2.402 with standard deviation of 0.12 Å. This is consistent with the upper limit root-mean-square (RMS) coordinate error of ~0.2 Å typical for structures obtained at this resolution. The Mn—O* bond lengths found in the crystal structure are exceptionally long for a hydroxide bridge and more consistent with the presence of a bridging water molecule. Given the much smaller uncertainty in the computed coordination bond lengths and the fact that the Mn—O* distance in the hydroxide model is clearly outside the range of variation found in the crystal structure, we support the notion of a water molecule occupying the bridging position. Evidence from EPR and EXAFS experiments can also be interpreted to support the above observation[14,16,17]: (1) The small value of the antiferromagnetic coupling constant J obtained from EPR points to a μ-H_2O rather than μ-OH ligand, and (2) the absence of detectable Mn–Mn EXAFS scattering was attributed to absence of a strongly bound ligand such as O^{2-} or OH^- in the binuclear metal cluster. Of course, caution should be used in comparing to experiments done at different values of pH, especially since our calculations indicate very similar thermodynamic stability for hydroxide and water in the active

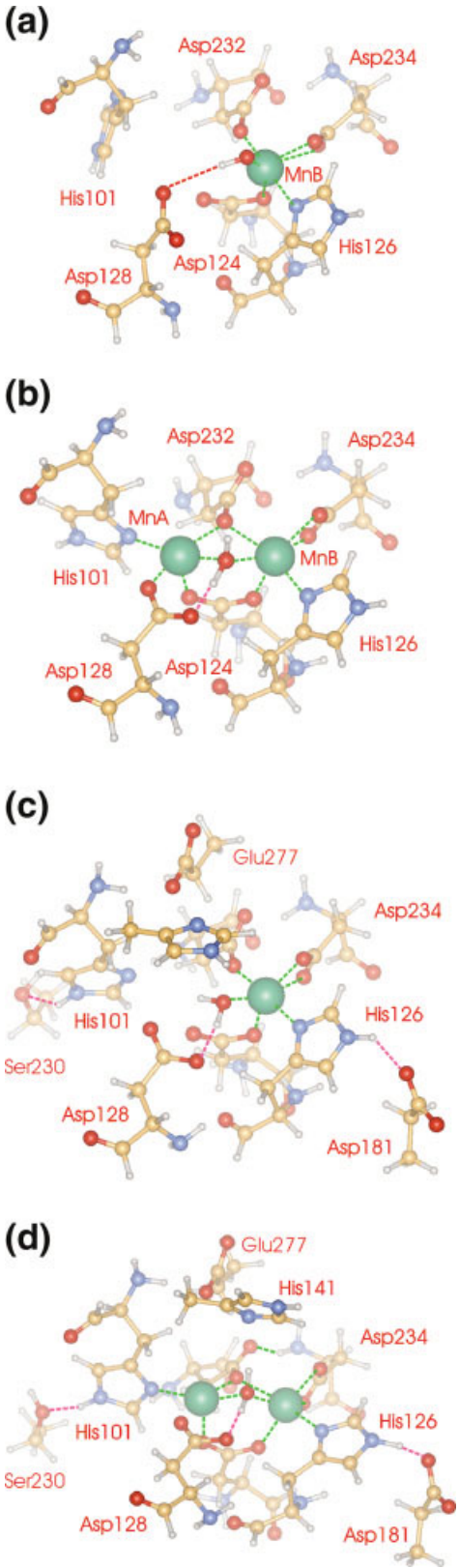

Fig. 2. Minimal models of the arginase active site: (**a**) Model RLA_dep; (**b**) Model RLA_h2o. Extended models of the arginase active site: (**c**) Model RLA_dep_ex ; (**d**) Model RLA_h2o_ex. Hydrogen bonds and coordination bonds are indicated by dashed lines.

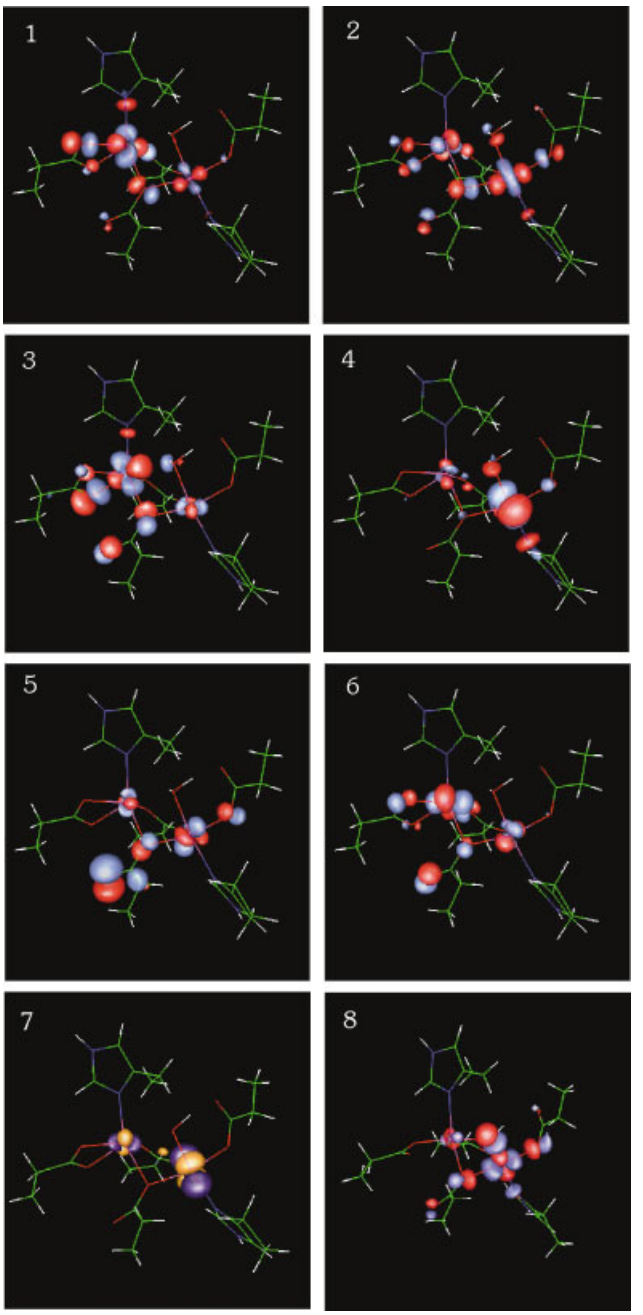

Fig. 3. Isodensity surface plots of the wavefunctions for select molecular orbitals in models RLA_h2o (**1–7**) and RLA_oh (**8**). The contours are drawn at values of ± 0.05; the negative and positive lobes of the wavefunctions are shown in blue and red, respectively, except for the lowest unoccupied β orbital of model RLA_h2o, shown in orange and violet. The plots **1–6** correspond to occupied spin-α orbitals ordered consecutively by decreasing energy from the highest occupied orbital (**1**). Plots **7** and **8** depict the lowest unoccupied β orbitals for RLA_h2o and RLA_oh, respectively.

site. Free energy simulations with ab initio molecular dynamics can be used to determine the pKa of a water molecule in the bridging position and resolve this issue without reference to experimental data. Such calculations are under way and will be reported separately.

For the minimal models with intact dimetal center, the basic structural features and the coordination polyhedra

TABLE I. Description of the Various QM Models of the Rat Liver Arginase Active Site

Model	N atoms	$V^{1/3}$ cell (Å)	2nd shell ligands	Mn atoms	Exogenous ligand
RLA_oh	98	16.52	No	2	OH^-
RLA_h2o	99	16.51	No	2	H_2O
RLA_dep	97	16.51	No	1	OH^-
RLA_h2o_ex	140	18.92	Yes	2	H_2O
RLA_dep_ex	145	18.92	Yes	1	H_2O
RLA_h2o_ex_sp	119	17.55	No	2	H_2O

All structures included the complete first shell ligands (capped and anchored at the peptide bond N, O, and C atoms). For the more extended models, a number of second shell ligands were added, and those were truncated at the β carbon atom and capped with hydrogens to achieve valence saturation. The extended and metal depleted models are denoted by the abbreviations ex and dep, respectively; sp denotes a model with protonated Asp181.

TABLE II. Characteristic Bond Lengths of Different QM Models of the Rat Liver Arginase Active Site

Distance (Å)	X-ray	RLA_h2o	RLA_oh	RLA_dep	RLA_h2o_ex	RLA_dep_ex	RLA_h2o_ex_sp
Mn_A–Nδ(His101)	2.24	2.14	2.15		2.12		2.13
Mn_B–Nδ(His126)	2.09	2.29	2.39	2.13	2.20	2.12	2.26
Mn_A–O1(Asp124)	2.03	2.02	2.07		2.04		2.00
Mn_B–O2(Asp124)	2.05	2.07	2.15	2.01	2.11	1.95	2.07
Mn_A–O* (H_2O/OH^-)		2.32	1.99		2.23		2.32
Mn_B–O* (H_2O/OH^-)		2.47	2.05	1.81	2.58	2.12	2.48
O*–O1(Asp128)		2.54	2.96	4.55	2.59	2.74	2.54
O(Ser230)–Nε(His101)	2.75				2.85	3.03	2.74
O(Asp181)–Nε(His126)	3.25				2.54	2.95	3.09
Mn_A–O(Asp232)	2.46	2.11	2.31		2.16		2.12
Mn_B–O(Asp232)	2.29	2.24	2.25	1.89	2.36	1.87	2.25
Mn_B–O1(Asp234)	2.11	2.15	2.10	2.14	2.10	1.98	2.12
Mn_B–O2(Asp234)	2.39	2.31	2.62	3.32	2.41	2.67	2.32
Mn_A–Mn_B	3.32	3.34	3.12		3.45		3.33

The corresponding distances in the X-ray structure of native rat liver arginase are listed in column 2 for comparison.

for Mn_A (square pyramidal geometry) and Mn_B (distorted octahedral geometry) are preserved. By contrast, in the minimal metal-depleted model, we observe a shift of the more distant O atom of the chelating Asp234 residue away from Mn_B. This transformation leaves the manganese center pentacoordinated in approximately square pyramidal geometry. It should be noted that a similar increase in the Mn_B—O2(Asp234) bond length is observed in the crystal structure of metal depleted arginase reported by Scolnick et al.[15] The Mn–O2 distance of ~2.6 Å found in the metal-depleted X-ray structure is larger than the corresponding distance in the metal-loaded form of the enzyme by about 0.2 Å. The limited resolution of the X-ray experiment in this case does not preclude the possibility of such deviation occurring at random. However, the increase in bond length is observed consistently and with similar magnitude in all three subunits of arginase, which renders this possibility highly unlikely. Despite the weakened binding, Asp234 remains a bidentate ligand in the crystal structure as opposed to our minimal model, where it is monodentate. It is likely that such difference in the mode of binding is a result of the limited size of our computational model. To corroborate this hypothesis, we studied an extended model of metal-depleted arginase in which the Asp181–His126 hydrogen bonding interaction fine-tunes the binding of the other ligands coordinated to Mn_B. In this case, the calculated distance between Mn_B and O2 of Asp234 is 2.67 Å, in very good agreement with experiment. Thus, the lengths of all coordination bonds are reproduced reasonably well by the extended model with one exception—the bond between Mn_B and the oxygen of Asp232. This bond length is larger by about 0.5 Å in the crystal structure—a deviation that may be too significant to explain by either the accuracy of the geometry optimization procedure or by the resolution of the X-ray structure. The fact that both the minimal and the extended models fail to reproduce this distance indicates that the models may be lacking specific hydrogen-bonding interactions or steric constraints that would prevent Asp232 from approaching closely the manganese atom. The corresponding distances in the crystal structure indicate a weaker coordination and display a certain level of disorder between the identical subunits (d Mn_B–O1(Asp232) = 2.29, 2.44, and 2.53 Å). Although qualitatively consistent with the X-ray structure, the minimal models show differences in several important details. Relatively large deviations in the orientation of His101, 126 were observed in the annealing trajectories, especially for the metal-depleted case. This is due to the lack of stabilizing hydrogen-bond interactions between the histidine residues and their respective second shell hydrogen-bonding partners. A significant rotation of the Asp128 residue is also found in the minimal metal

depleted model (RLA_dep). The substantial improvement in several key structural parameters with the inclusion of Ser230 and Asp181 residues in our extended models (RLA_dep_ex, RLA_h2o_ex; see Fig. 2) underscores the importance of second shell interactions in determining the structure of the active site. It is also interesting to note that hydrogen bonding with Asp181 tends to reinforce the bond between Mn_B and the Nδ atom of His126. Correspondingly, the bond length is shorter by 0.09 Å in the extended (RLA_h2o_ex) compared to the minimal (RLA_h2o) model. Protonation of Asp181 (RLA_h2o_ex_sp) decreases the magnitude of the effect but does not eliminate it ($\Delta d = 0.03$ Å). This observation is consistent with the idea that Asp181 confers a partial histidinato-like character to the His126 residue, which may thus indirectly influence the coordination of the bridging nucleophile. By contrast, hydrogen bonding to Ser230 at the opposite end of the active site has no effect on the coordination of His101 to Mn_A. Hydrogen bonding to the aspartate residues is also important for maintaining the structural integrity of the active site. Our extended models faithfully reproduce some of these interactions. For instance, the dangling oxygen atom of Asp232 forms an antioriented H-bond with the backbone NH of Asp234, and Asp 234 in turn participates in a hydrogen bond with the Asp124 residue.

The exogenous ligand, either a water molecule or a hydroxide anion, was found to readily coordinate to the dimetal center. In the case of hydroxide, it assumes a symmetric bridging position almost equidistant from both manganese cations. The asymmetry in terms of bond distances is much more pronounced in the case of H2O, reflecting the somewhat weaker binding of this ligand. In all relevant models the Mn_A—O* distances are consistently shorter (see Table I). The solvent molecule (H2O or OH−) was observed to move significantly from its initial position to form a hydrogen bond with the dangling oxygen of Asp128—a residue implicated as catalytically important. The H-bond is especially strong in the case of a water bridge, with short distances between the donor and acceptor atoms and an angle between the atoms close to 180° [d(O*—O) = 2.54 Å; d(O*—H) = 1.06 Å; d(H···O) = 1.50 Å; angle (O*—H···O) = 168.22°]. For this reason, Asp128 can be identified as one of the candidates for the deprotonation of an incoming bridging water molecule in the final step of the catalytic cycle [see Fig. 2(b)]. The above hydrogen-bonding interaction is analogous to the one observed in a recently synthesized binuclear biomimetic compound that exhibits a strong hydrogen bond between a solvent molecule and a carboxylate in the same orientation for a series of metals residing in the bridged binuclear motif (Ni^{2+}, Co^{2+}, Co^{3+}, and Zn^{2+}).[18] The strong hydrogen bonding between the bridging water molecule and the terminal monodentate Asp128 residue may serve a dual purpose. First, it may facilitate the formation of the active nucleophile OH^- through proton transfer along the O—H···O coordinate. Second, the decreased ability of the resulting protonated aspartate to stabilize the positive charge on Mn_A may result in increased Lewis acidity at the metal cluster. Interestingly, the hydrogen bond between Asp128 and the bridging solvent molecule is maintained even in the absence of Mn_A, as is the case of our extended metal depleted model. This may explain why the metal-depleted variant of the enzyme retains partial catalytic activity.

By carrying out Mulliken population analysis, we confirmed that the predominantly negatively charged ligands provide strong electrostatic stabilization for the manganese ions. The charge on both Mn_A and Mn_B is reduced from the formal value of +2 e to approximately +1 e (+1.02 e (Mn_A) and +0.92 e (Mn_B) for the RLA_h2o model; +1.04 e (Mn_A) and +0.96 e (Mn_B) for the RLA_oh model). The rest of the positive charge is thus distributed over the ligands. Especially important in this role are the negatively charged aspartate residues. Moreover, both the Mulliken and Hirshfeld charge partitioning schemes indicate the nonequivalence of the manganese atoms in terms of charge. Mn_A carries about 10% larger positive charge compared to Mn_B, reflecting a somewhat smaller electrostatic stabilization by the coordinating negatively charged ligands. This makes it the more likely center on which the nucleophilic hydroxide ion could be localized if it is released from its stable bridging position.

An electronic structure analysis on two minimal models reveals a rather complicated picture of the bonding in the active site of arginase. In order to simplify the annotation of the orbitals, the models were further reduced to exclude the peptide bond nitrogen and oxygen atoms. The nonbonding orbitals located on these atoms unnecessarily complicate the molecular orbital picture close to the energy gap. The Kohn–Sham eigenvalues for 10 occupied spin-α and spin-β orbitals, and 5 unoccupied spin-α and spin-β orbitals are included as supplemental information for two models: RLA_h2o and RLA_oh. The energy diagram shows energy gaps between the highest occupied and lowest unoccupied molecular orbitals of 2.88 eV and 2.44 eV, respectively. The apparent shift in the in the energy levels for the RLA_h2o model with respect to the other model is due to the difference in total charge. Visual inspection of isosurface plots (see Fig. 3) of the occupied spin-α orbitals close to the HOMO-LUMO gap reveals that these molecular orbitals are highly delocalized and involve contributions from the aspartate oxygen atoms, the bridging solvent molecule (H2O) and the 3d atomic orbitals on Mn_A and Mn_B. It is important to note that orbitals involving the atoms of the terminal aspartate Asp234 ligand, as well as the flexible μ -1,1 bridging Asp232, lie at high energies close to the gap. This observation is consistent with weak coordination of these residues and suggests them as departing ligands should any rearrangements occur in the active site. Very recent crystallographic data on human arginase II has shown structural variability in the position of the residue analogous to Asp232, which is consistent with our findings.[19] In contrast to the occupied spin-α orbitals, the unoccupied spin-α and spin-β orbitals are mostly localized: the former on the manganese centers and the latter on the aromatic π system of the imidazole rings. The presence of low-lying unoccupied orbitals on the metal atoms has influence on the redox properties of arginase, as well as affects the possibility of substrate, inhibitor, or product binding.[20] Models with substrate docked in the

active site are presently being investigated and will be reported in a separate article.

METHODS

In the present study, we have employed spin-unrestricted DFT methodology based on the local spin density (LSD) approximation. A systematic investigation of a number of models for the active site of rat liver arginase was carried out using a combination of simulated annealing and geometry optimization. The models constructed differed in the number of ligands included, number of metal centers, presence of second shell ligands or substrate, and the protonation state of the exogenous ligand. The geometry optimizations were performed with the program CPMD.[22,23] The gradient corrected exchange-correlation functional of Becke and Perdew (BP)[24,25] was selected for the present study. To account for the valence–core interactions, we employed an analytical von Barth and Car pseudopotential for hydrogen and norm-conserving Troullier–Martins pseudopotentials[26] for all other elements. The valence electronic wavefunctions were expanded in a plane wave basis set with an energy cutoff of 100 Ry. All hydrogen nuclei were replaced by deuterium. In addition, the mass of Mn was rescaled to half its value to accelerate phase space sampling in the simulated annealing runs. A fictitious electronic mass of 900 a.u. was selected, which enabled integration of the equations of motion with a timestep of 0.150 fs (6.0 a.u.). Cluster boundary conditions were employed, and the periodic images were decoupled using the method of Hockney.[27] Ferromagnetic coupling of the manganese ions was enforced for all models by fixing the multiplicity of the manganese atoms to the highest possible value. The validity of this approximation is based on the assumption of weak coupling between the metal centers and has been verified by others.[28,29]

Additional single-point calculations utilizing the B3LYP[25,30] exchange-correlation functional were performed to determine the electrostatic properties and electronic structure of the active site. We employed the DZVP2(DFT_Orbital) basis set[31] in combination with the corresponding Coulomb and exchange-fitting basis sets (DGauss_A2 DFT Coulomb-Fitting; DGauss_A2 DFT Exchange-Fitting). The program NWChem[32] was used to carry out these calculations.

CONCLUSIONS

In summary, we have carried out computationally demanding DFT calculations on realistic models of the rat liver arginase active site. Based on the optimized structures, we have identified the bridging exogenous ligand to be a water molecule rather than hydroxide ion. Unlike hydroxide, the water molecule is asymmetrically bridging with pronounced preference for stronger binding to Mn_A in all relevant models. It was also determined that the two manganese atoms are nonequivalent in terms of charge and local electrostatic potential. This may have mechanistic implications, since the two proposed mechanisms differ with respect to the nature of the nucleophilic attack—from terminal versus bridging position. Second shell ligands were shown to be important in fine-tuning the interactions between the dimetal center and the first shell ligands. Most notably, hydrogen bonding to the histidine ligands (His101 and His126) helps to orient these residues in the active site and in the case of His 126 modulates the length of the Mn—Nδ bond. The Asp128 residue was identified as a likely deprotonating group for the bridging nucleophile based on the formation of a strong short hydrogen bond, which is preserved even in the metal-depleted form. This may explain the partial activity of the metal-deficient form of the enzyme. Finally, electronic structure analysis revealed that orbitals involving the terminal Asp234 and the monodentate bridging Asp232 lie at high energies, suggesting them as potential departing ligands, in agreement with recent experimental findings.[19,21]

ACKNOWLEDGMENTS

We thank Prof. David Christianson for helpful comments and for sharing his preliminary results with us. We also thank Alessandra Magistrato, Petra Munih, and Robert Doerksen for many stimulating discussions. Computer resources were provided, in part, by the Pittsburgh Supercomputing Center through NPACI. The software package NWChem Version 4.1, as developed and distributed by Pacific Northwest National Laboratory, P. O. Box 999, Richland, Washington 99352, and funded by the U. S. Department of Energy, was used to obtain part of the results.

REFERENCES

1. Wilcox DE. Binuclear metallohydrolases. Chem Rev 1996;96:2435–2458.
2. Pelletier H, Sawaya MR, Kumar A, Wilson SH, Kraut J. Structures of ternary complexes of rat DNA polymerase b, a DNA template-primer and ddCTP. Science 1994;264:1891–1903.
3. Klabunde T, Sträter N, Fröhlich R, Witzel H, Krebs B. Mechanism of Fe(III)-Zn(II) purple acid phosphatase based on crystal structures. J Mol Biol 1996;259:737–748.
4. Kim EE, Wyckoff HW. Reaction mechanism of alkaline phosphatase based on crystal structures. J Mol Biol 1991;218:449–464.
5. Sträter N, Lipscomb WN. Two-metal ion mechanism of bovine lens leucine aminopeptidase: active site solvent structure and binding mode of L-leucinal, a gem-diolate transition state analogue, by X-ray crystallography. Biochemistry 1995;34:14792–14800.
6. Wilce MCJ, Bond HS, Dixon NE, Freeman HC, Guss JM, Lilley PE, Wilce JA. Structure and mechanism of a proline-specific aminopeptidase from *Escherichia coli*. Proc Natl Acad Sci USA 1998;95:3472–3477.
7. Jordan A, Reichard P. Ribonucletide reductases. Annu Rev Biochem 1999;67:71–98.
8. Wallar BJ, Lipscomb JD. Dioxygen activation by enzymes containing binuclear non-heme iron clusters. Chem Rev 1996;96:2625–2657.
9. Barynin V, Whittaker MM, Antonyuk SV, Lamzin VS, Harrison PM, Artymiuk PJ, Whittaker JW. Crystal structure of manganese catalase from *Lactobacillus plantarum*. Structure 2001;9:725–738.
10. Christianson DW. Structural chemistry and biology of manganese metalloenzymes. Prog Biophys Mol Biol 1997;67:217–243.
11. Christianson DW, Cox JD. Catalysis by metal-activated hydroxide in zinc and manganese metalloenzymes. Annu Rev Biochem 1999;68:33–57.
12. Ash DE, Cox JD, Christianson DW. Arginase: a binuclear manganese metalloenzyme. Metal Ions Biol Syst 2000;37:407–428.
13. Kanyo ZF, Scolnick LR, Ash DE, Christianson DW. Structure of a unique binuclear manganese cluster in arginase. Nature 1996;383:554–557.
14. Khangulov SV, Sossong TM, Ash DE, Dismukes GC. L-arginine binding to liver arginase requires proton transfer to gateway

residue His141and coordination of the guanidinium group to the dimanganese(II,II) center. Biochemistry 1998;37:8539–8550.
15. Scolnick LR, Kanyo ZF, Cavalli RC, Ash DE, Christianson DW. Altering the binuclear manganese cluster of arginase diminishes thermostability and catalytic function. Biochemistry 1997;36: 10558–10565.
16. Khangulov SV, Pessiki PJ, Barynin VV, Ash DE, Dismukes GC. Determination of the metal-ion separation and energies of the 3 lowest electronic states of dimanganese (II,II) complexes and enzymes—catalase and liver arginase. Biochemistry 1995;34: 2015–2025.
17. Stemmler TL, Sossong TM, Goldstein JI, Ash DE, Elgren TE, Krutz DM, PennerHahn JE. EXAFS comparison of the dimanganese core structures of manganese catalase, arginase, and manganese-substituted ribonucleotide reductase and hemerythrin. Biochemistry 1997;36:9847–9858.
18. Lee D, Hung PL, Spingler B, Lippard SJ. Sterically hindered carboxylate ligands support water-bridged dimetallic centers that model features of metallohydrolase active sites. Inorg Chem 2002;4:521–531.
19. Cama E, Colleluori DM, Emig FA, Shin H, Kim SW, Kim NN, Traish AM, Ash DE, Christianson DW. Human arginase II: Crystal structure and physiological role in male and female sexual arousal. Biochemistry 2003;42:8445–8451.
20. Cox JD, Cama E, Colleluori DM, Pethe S, Boucher JL, Mansuy D, Ash DE, Christianson DW. Mechanistic and metabolic inferences from the binding of substrate analogues and products to arginase. Biochemistry 2001;40:2689–2701.
21. Cama E, Ernig FA, Ash DE, Christianson DW. Structural and functional importance of first-shell metal ligands in the binuclear manganese cluster of arginase I. Biochemistry 2003;42:7748–7758.
22. Car R, Parrinello M. Unified approach for molecular-dynamics and density-functional theory. Phys Rev Lett 1985;55:2471–2474.
23. Hutter J, Alavi A, Deutsch T, Bernasconi M, Goedecker S, Marx D, Tuckerman M, Parrinello M. CPMD version 3.4. Stuttgart and Zurich: MPI für Festkörperforschung and IBM Research Laboratory; 1995–2000.
24. Perdew JP. Density-functional approximation for the correlation-energy of the inhomogeneous electron-gas. Phys Rev B 1986;33: 8822–8824.
25. Becke AD. Density-functional exchange-energy approximation with correct asymptotic behavior. Phys Rev A 1988;38:3098–3100.
26. Troullier N, Martins JL. Efficient pseudopotentials for plane-wave calculations. Phys Rev B 1991;43:1993–2006.
27. Hockney RW. The potential calculation and some applications. Methods Comput Phys 1970;9:135–211.
28. Siegbahn PEM. Quantum chemical studies of manganese centers in biology. Curr Opin Chem Biol 2002;6:227–235.
29. Blomberg MRA, Siegbahn PEM. A quantum chemical approach to the study of reaction mechanisms of redox-active metalloenzymes. J Phys Chem B 2001;105:9375–9386.
30. Lee CT, Yang WT, Parr RG. Development of the Colle–Salvetti correlation-energy formula into a functional of the electron-density. Phys Rev B 1988;37:785–789.
31. Godbout N, Salahub DR, Andzelm J, Wimmer E. Optimization of Gaussian type basis sets for local spin-density functional calculations: 1. Boron through neon, optimization technique and validation. Can J Chem 1992;70:560–571.
32. High Performance Computational Chemistry Group. NWChem, a computational chemistry package for parallel computers, Version 4.1. Richland, WA: Pacific Northwest National Laboratory; 2002.